



1 Nitrate-driven haze pollution during summertime over the North China 2 Plain

3 Haiyan Li¹, Qiang Zhang², Bo Zheng³, Chunrong Chen², Nana Wu², Hongyu Guo⁴, Yuxuan Zhang², Yixuan
4 Zheng², Xin Li², Kebin He^{1,5}

5 ¹ State Key Joint Laboratory of Environment Simulation and Pollution Control, School of Environment, Tsinghua University,
6 Beijing 100084, China

7 ² Ministry of Education Key Laboratory for Earth System Modeling, Department of Earth System Science, Tsinghua University,
8 Beijing 100084, China

9 ³ Laboratoire des Sciences du Climat et de l'Environnement, CEA-CNRS-UVSQ, UMR8212, Gif-sur-Yvette, France

10 ⁴ School of Earth and Atmospheric Sciences, Georgia Institute of Technology, Atlanta, GA, 30332, USA

11 ⁵ State Environmental Protection Key Laboratory of Sources and Control of Air Pollution Complex, Tsinghua University, Beijing
12 100084, China

13 *Correspondence to:* Qiang Zhang (qiangzhang@tsinghua.edu.cn) or Kebin He (hekb@tsinghua.edu.cn)

14 **Abstract.** Compared to the severe winter haze episodes in the North China Plain (NCP), haze pollution during summertime has
15 drawn little public attention. In this study, we present the highly time-resolved chemical composition of submicron particles (PM₁)
16 measured in Beijing and Xinxiang in the NCP region during summertime to evaluate the driving factors of aerosol pollution.
17 During the campaign periods (30 June to 27 July, 2015, for Beijing and 8 to 25 June, 2017, for Xinxiang), the average PM₁
18 concentrations were 35.0 $\mu\text{g m}^{-3}$ and 64.2 $\mu\text{g m}^{-3}$ in Beijing and Xinxiang, respectively. Pollution episodes characterized with
19 largely enhanced nitrate concentrations were observed at both sites. In contrast to the slightly decreased mass fractions of sulfate,
20 semi-volatile oxygenated organic aerosol (SV-OOA), and low-volatile oxygenated organic aerosol (LV-OOA) in PM₁, nitrate
21 displayed an almost linearly increased contribution with the aggravation of aerosol pollution in both Beijing and Xinxiang,
22 highlighting the importance of nitrate formation as the driving force of haze evolution in summer. Rapid nitrate production mainly
23 occurred after midnight, with a higher formation rate than that of sulfate, SV-OOA, or LV-OOA. Detailed investigation of nitrate
24 behaviors revealed several factors influencing the rapid nitrate formation in summer: high ammonia emissions in the NCP region,
25 the gas-to-particle equilibrium of ammonium nitrate closely related to variations in temperature and relative humidity, nighttime
26 nitrate production through heterogeneous hydrolysis of dinitrogen pentoxide (N₂O₅), and regional transport from different air mass
27 origins. Finally, atmospheric particulate nitrate data acquired by mass spectrometric techniques from various field campaigns in
28 Asia, Europe, and North America uncovered a higher concentration and higher fraction of nitrate present in China. Although
29 measurements in Beijing during different years demonstrate a decline in the nitrate concentration in recent years, the nitrate
30 contribution in PM₁ still remains high. To effectively alleviate particulate matter pollution in summer, our results call for the urgent
31 need to initiate ammonia emission control measures and further reduce nitrogen oxide emissions over the NCP region.

32 1 Introduction

33 Atmospheric aerosol particles are known to significantly impact visibility (Watson, 2002) and human health (Pope et al., 2009;
34 Cohen et al., 2017), as well as affect climate change by directly and indirectly altering the radiative balance of Earth's atmosphere
35 (IPCC, 2007). The effects of aerosols are intrinsically linked to the chemical composition of particles, which are usually dominated
36 by organics and secondary inorganic aerosols (i.e., sulfate, nitrate, and ammonium) (Jimenez et al., 2009).

37 In recent years, severe haze pollution has repeatedly struck the North China Plain (NCP), and its effects on human health have
38 drawn increasing public attention. Correspondingly, the chemical composition, sources, and evolution processes of particulate



39 matter (PM) have been thoroughly investigated (Huang et al., 2014; Guo et al., 2014; Cheng et al., 2016; Li et al., 2017a), mostly
40 during extreme pollution episodes in winter. Unfavorable meteorological conditions, intense primary emissions from coal
41 combustion and biomass burning, and fast production of sulfate through heterogeneous reactions were found to be the driving
42 factors of heavy PM accumulation in the NCP region (Zheng et al., 2015; Li et al., 2017b; Zou et al., 2017). Although summer is
43 characterized by relatively better air quality compared to the serious haze pollution in winter, fine particle (PM_{2.5}) concentration
44 in the NCP region still remains high during summertime. Through one-year real-time measurements of non-refractory submicron
45 particles (NR-PM₁), Sun et al. (2015) showed that the aerosol pollution during summer was comparable to that during other seasons
46 in Beijing, and the hourly maximum concentration of NR-PM₁ during the summer reached over 300 µg m⁻³. Previous studies
47 focusing on the seasonal variations of aerosol characteristics have noted quite different behaviors of aerosol species in winter and
48 summer (Hu et al., 2017). Therefore, figuring out the specific driving factors of haze evolution in summer would help establish
49 effective air pollution control measures.

50 Compared to more than 70% reduction of sulfur dioxide (SO₂) emissions since 2006 due to the wide application of flue-gas
51 desulfurization devices in power plants and the phase-out of small, high emitting power generation units (Li et al., 2017c), nitrogen
52 oxide (NO_x) emissions in China remain high and decreased by less than 20% from 2012 to 2015 (Liu et al., 2016). Therefore, the
53 role of nitrate formation in aerosol pollution is predicted to generally increase as a consequence of high ammonia (NH₃) emissions
54 in the NCP region. However, due to the significantly enhanced production of sulfate in extreme winter haze resulting from the
55 high relative humidity (RH) and large SO₂ emissions from coal combustion, little attention has been paid to nitrate behaviors. In
56 PM_{2.5}, aerosol nitrate mostly exists in the form of ammonium nitrate, via the neutralization of nitric acid (HNO₃) with NH₃. HNO₃
57 is overwhelmingly produced through secondary oxidation processes, NO₂ oxidized by OH during the day and hydrolysis of N₂O₅
58 at night, with the former being the dominant pathway (Alexander et al., 2009). The neutralization of HNO₃ is limited by the
59 availability of NH₃, as NH₃ prefers to react first with sulfuric acid (H₂SO₄) to form ammonium sulfate with lower volatility
60 (Seinfeld and Pandis, 2006). Because ammonium nitrate is semi-volatile, its formation also depends on the gas-to-particle
61 equilibrium, which is closely related to variations in temperature and RH. A recent review on PM chemical characterization
62 summarized that aerosol nitrate accounts for 16~35% of submicron particles (PM₁) in China (Li et al., 2017a). Some studies also
63 pointed out the importance of aerosol nitrate in haze formation in the NCP region (Sun et al., 2012; Yang et al., 2017). However,
64 detailed investigations and the possible mechanisms governing nitrate behaviors during pollution evolution are still very limited.
65 In this study, we present in-depth analysis of the chemical characteristics of PM₁ at urban sites in Beijing and Xinxiang, China
66 during summertime. Based on the varying aerosol composition with the increase of PM₁ concentration, the driving factors of haze
67 development were evaluated, and the significance of nitrate contribution was uncovered. In particular, we investigated the chemical
68 behavior of nitrate in detail and revealed the factors favoring rapid nitrate formation during summer in the NCP region.

69 2 Experiments

70 2.1 Sampling site and instrumentation

71 The data presented in this study were collected in Beijing from 30 June to 27 July, 2015, and in Xinxiang from 8 to 25 June, 2017.
72 Beijing is the capital city of China, adjacent to Tianjin municipality and Hebei province, both bearing high emissions of air
73 pollutants. The Beijing-Tianjin-Hebei region is regularly listed as one of the most polluted areas in China by the China National
74 Environmental Monitoring Centre. The field measurements in Beijing were performed on the roof of a three-floor building on the
75 campus of Tsinghua University (40.0 °N, 116.3 °E). The sampling site is surrounded by school and residential areas, and no major
76 industrial sources are located nearby. Xinxiang is a prefecture-level city in northern Henan province, characterized by considerable



77 industrial manufacturing. In February 2017, the Chinese Ministry of Environmental Protection issued the “Beijing-Tianjin-Hebei
78 and the surrounding areas air pollution prevention and control work program 2017” to combat air pollution in Northern China. The
79 action plan covers the municipalities of Beijing and Tianjin and 26 cities in Hebei, Shanxi, Shandong and Henan provinces, referred
80 to as “2+26” cities. Xinxiang is listed as one of the “2+26” cities. The average $PM_{2.5}$ concentrations in Xinxiang in 2015 and 2016
81 were $94 \mu g m^{-3}$ and $84 \mu g m^{-3}$, respectively. Our sampling in Xinxiang was performed in the mobile laboratory of Nanjing
82 University, deployed in the urban district near an air quality monitoring site ($35.3^{\circ} N$, $113.9^{\circ} E$).
83 An Aerodyne Aerosol Chemical Speciation Monitor (ACSM) was deployed for the chemical characterization of NR- PM_1 , with a
84 time resolution of 15 minutes. Briefly, ambient aerosols were sampled into the ACSM system at a flow rate of $3 L min^{-1}$ through
85 a $PM_{2.5}$ cyclone to remove coarse particles and then a silica gel diffusion dryer to keep particles dry ($RH < 30\%$). After passing
86 through a $100 \mu m$ critical orifice mounted at the entrance of an aerodynamic lens, aerosol particles with a vacuum aerodynamic
87 diameter of ~ 30 -1000 nm were directly transmitted into the detection chamber, where non-refractory particles were flash vaporized
88 at the oven temperature ($\sim 600^{\circ} C$) and chemically characterized by 70 eV electron impact quadrupole mass spectrometry. Detailed
89 descriptions of the ACSM technique can be found in Ng et al. (2011). The mass concentration of refractory BC in PM_1 was recorded
90 by a multi-angle absorption photometer (MAAP Model 5012, Thermo Electron Corporation) on a 10-min resolution basis (Petzold
91 and Schönlinner, 2004; Petzold et al., 2005). The MAAP was equipped with a PM_1 cyclone, and a drying system was incorporated
92 in front of the sampling line. A suite of commercial gas analyzers (Thermo Scientific) were also deployed to monitor variations in
93 the gaseous species (i.e., CO, O₃, NO, NO_x, and SO₂).
94 For observations in Beijing, the total PM_1 mass was simultaneously measured using a PM-714 Monitor (Kimoto Electric Co., Ltd.,
95 Japan) based on the β -ray absorption method (Li et al., 2016). Meteorological conditions, including temperature, RH, wind speed,
96 and wind direction, were reported by an automatic meteorological observation instrument (Milos520, VAISALA Inc., Finland).
97 For measurements in Xinxiang, the online $PM_{2.5}$ mass concentration was measured using a heated Tapered Elemental Oscillating
98 Microbalance (TEOM series 1400a, Thermo Scientific). The temperature and RH were obtained using a Kestrel 4500 Pocket
99 Weather Tracker.

100 2.2 ACSM data analysis

101 The mass concentrations of aerosol species, including organics, sulfate, nitrate, ammonium, and chloride, can be determined from
102 the ion signals detected by the quadrupole mass spectrometer (Ng et al., 2011) using the standard ACSM data analysis software
103 (v.1.5.3.0) within Igor Pro (WaveMetrics, Inc., Oregon USA). Default relative ionization efficiency (RIE) values were assumed
104 for organics (1.4), nitrate (1.1), and chloride (1.3). The RIEs of ammonium and sulfate were determined to be 7.16 and 1.08,
105 respectively, through calibration with pure ammonium nitrate and ammonium sulfate. To account for the incomplete detection of
106 aerosol particles (Ng et al., 2011), a constant collection efficiency (CE) of 0.5 was applied to the entire dataset. After all the
107 corrections, the mass concentration of ACSM NR- PM_1 plus BC was closely correlated with that of total PM_1 obtained by PM-714
108 in Beijing ($r^2 = 0.59$; Fig. S1). The slope was slightly higher than 1, which was probably caused by different measuring methods
109 of the different instruments and the uncertainties. For measurements in Xinxiang, the mass concentration of ACSM NR- PM_1 plus
110 BC also displayed a good correlation with $PM_{2.5}$ concentration measured by TEOM, with a slope of 0.83 ($r^2 = 0.85$; Fig. S1).
111 Positive matrix factorization (PMF) with the PMF2.exe algorithm (Paatero and Tapper, 1994) was performed on ACSM organics
112 mass spectra to explore various sources of organic aerosol (OA). Only m/z 's up to 120 were considered due to the higher
113 uncertainties of larger m/z 's and the interference of the naphthalene internal standard at m/z 127-129. In general, signals with $m/z >$
114 120 only account for a minor fraction of total signals. Therefore, this kind of treatment has little effect on the OA source
115 apportionment. PMF analysis was performed with an Igor Pro-based PMF Evaluation Tool (PET) (Ulbrich et al., 2009), and the



116 results were evaluated following the procedures detailed in Ulbrich et al. (2009) and Zhang et al. (2011). According to the
117 interpretation of the mass spectra, the temporal and diurnal variations of each factor, and the correlation of OA factors with external
118 tracer compounds, a four-factor solution with FPEAK = 0 and a three-factor solution with FPEAK = 0 were chosen as the optimum
119 solutions in Beijing and Xinxiang, respectively. The total OA in Beijing was resolved into a hydrocarbon-like OA (HOA) factor,
120 a cooking OA (COA) factor, a semi-volatile oxygenated OA (SV-OOA) factor, and a less-volatile oxygenated OA (LV-OOA)
121 factor, where the former two represented primary sources, and the latter two came from secondary formation processes. In Xinxiang,
122 the identified OA factors included HOA, SV-OOA, and LV-OOA. Procedures for OA source apportionment are detailed in the
123 supplementary materials (Text S1; Tables S1-2; Figs. S2-7).

124 2.3 ISORROPIA-II equilibrium calculation

125 To investigate factors influencing the particulate nitrate formation, the ISORROPIA-II thermodynamic model was used to
126 determine the equilibrium composition of an NH_4^+ - SO_4^{2-} - NO_3^- - Cl^- - Na^+ - Ca^{2+} - K^+ - Mg^{2+} - water inorganic aerosol (Fountoukis
127 and Nenes, 2007). When applying ISORROPIA-II, we assumed that the aerosol was internally mixed and composed of a single
128 aqueous phase, and the bulk PM_1 or $\text{PM}_{2.5}$ properties had no compositional dependence on particle size. The validity of the model
129 performance for predicting particle pH, water, and semi-volatile species has been examined by a number of studies in various
130 locations (Guo et al., 2015, 2016, 2017a; Hennigan et al., 2015; Bougiatioti et al., 2016; Weber et al., 2016; Liu et al., 2017). In
131 this study, the sensitivity analysis of PM_1 nitrate formation to gas-phase NH_3 and PM_1 sulfate concentrations was performed using
132 the ISORROPIA-II model, running in the “forward mode” for a metastable aerosol state. Input to ISORROPIA-II includes the
133 average RH, T, and total NO_3^- ($\text{HNO}_3 + \text{NO}_3^-$) for typical summer conditions (RH = 56%, T = 300.21K) in Beijing and Xinxiang,
134 along with a selected sulfate concentration. Total NH_4^+ ($\text{NH}_3 + \text{NH}_4^+$) was left as the free variable. The variations in nitrate
135 partitioning ratio ($\varepsilon(\text{NO}_3^-) = \text{NO}_3^- / (\text{HNO}_3 + \text{NO}_3^-)$) were examined with varying sulfate concentrations from 0.1 to 45 $\mu\text{g m}^{-3}$ and
136 equilibrated NH_3 between 0.1 and 50 $\mu\text{g m}^{-3}$.

137 2.4 Air mass trajectory analysis

138 Back trajectory analysis using the Hybrid Single-Particle Lagrangian Integrated Trajectory (HYSPLIT) model (Draxler and Hess,
139 1998) was conducted to explore the influence of regional transport on aerosol characteristics in Beijing. The meteorological input
140 was adopted from the NOAA Air Resource Laboratory Archived Global Data Assimilation System (GDAS)
141 (<ftp://arlftp.arlhq.noaa.gov/pub/archives/>). The back trajectories initialized at 100 m above ground level were calculated every hour
142 throughout the campaign and then clustered into several groups according to their similarity in spatial distribution. In this study, a
143 four-cluster solution was adopted, as shown in Fig. S8.

144 3 Results and discussion

145 3.1 Overview of aerosol characteristics

146 Summer is usually the least polluted season of the year in the NCP region due to favorable weather conditions and lower emissions
147 from anthropogenic sources (Hu et al., 2017). Figures 1 and 2 show the time series of meteorological parameters, gaseous species
148 concentrations, and aerosol species concentrations in Beijing and Xinxiang. The weather during the two campaigns was relatively
149 hot (average T = 27.1 ± 4.1 °C for Beijing and 26.9 ± 4.0 °C for Xinxiang) and humid (average RH = $55.9 \pm 18.5\%$ for Beijing
150 and $63.5 \pm 17.2\%$ for Xinxiang), with regular variations between day and night. The average PM_1 (= NR- PM_1 + BC) concentration



151 was $35.0 \mu\text{g m}^{-3}$ in Beijing and $64.2 \mu\text{g m}^{-3}$ in Xinxiang, with the hourly maximum reaching $114.9 \mu\text{g m}^{-3}$ and $208.1 \mu\text{g m}^{-3}$,
152 respectively. Several pollution episodes were clearly observed at the two sites, along with largely increased nitrate concentrations.
153 Secondary inorganic aerosol, including sulfate, nitrate, and ammonium, dominated the PM_1 mass with an average contribution
154 above 50%. The higher nitrate fraction (24% in Beijing and 26% in Xinxiang) is similar to previous observations during summer
155 (Sun et al., 2015; Hu et al., 2016), likely due to photochemical processes being more active than in winter. The mass fraction of
156 OA is lower than that measured during winter in the NCP region (Hu et al., 2016; Li et al., 2017b), in accordance with the large
157 reduction of primary emissions in summer. According to the source apportionment results, OA at both sites is largely composed
158 of secondary factors, in which 44-52% is LV-OOA and 22-23% is SV-OOA (Figs. S4-5). Primary organic aerosol accounts for
159 only 34% and 24% of the total OA in Beijing and Xinxiang, respectively. As there is no need for residential home-heating in
160 summer, which results in lower air pollutant emissions from coal combustion, chloride accounts for a smaller fraction of
161 approximately 1% in total PM_1 . In addition, the higher temperature during summer drives the partitioning of semi-volatile
162 ammonium chloride into the gas phase, leading to lower concentrations of chloride in the particle phase.
163 The diurnal variations of aerosol species are similar in the measurements from Beijing and Xinxiang (Fig. S9). Organics
164 demonstrated two pronounced peaks at noon and in the evening. Source characterization of OA suggested that the noon peak was
165 primarily driven by cooking emissions, while the evening peak was a combination of various primary sources, i.e., traffic and
166 cooking. Relatively flat diurnal cycles were observed for sulfate, suggesting that the daytime photochemical production of sulfate
167 may be masked by the elevated boundary layer height after sunrise. Nitrate displayed lower concentrations in the afternoon and
168 higher values at night. To eliminate the effects of different dilution/mixing conditions with the development of boundary layer
169 height, diurnal patterns of the nitrate/sulfate ratio were analyzed to determine the role of chemical processes on nitrate behavior.
170 The nitrate/sulfate ratio showed the lowest value at approximately 4 pm, indicating that the evaporative loss of particulate NH_4NO_3
171 into gaseous NH_3 and HNO_3 overcame its photochemical production. The nitrate/sulfate ratio peaked at night, revealing the
172 significance of nighttime nitrate formation. During the night, nitrate production is mainly controlled by the heterogeneous
173 hydrolysis of N_2O_5 (Pathak et al., 2011), which is favored at high RH. A recent study conducted in urban Beijing observed high
174 N_2O_5 concentrations during pollution episodes and highlighted the vital role of N_2O_5 chemistry in nitrate formation (Wang et al.,
175 2017).

176 3.2 Enhancement of nitrate formation during pollution episode

177 To effectively mitigate aerosol pollution through policy-making, the driving factors of the PM increase need to be determined.
178 Figure 3 illustrates the mass contributions of various species in PM_1 as a function of PM_1 concentration in Beijing and Xinxiang.
179 OA dominated PM_1 at lower mass loadings ($> 40\%$ when $\text{PM}_1 < 20 \mu\text{g m}^{-3}$), but its contribution significantly decreased with
180 increased PM_1 concentration. The source apportionment of OA demonstrated that the large reduction in OA fraction was primarily
181 driven by POA, especially in Beijing. The contribution of SV-OOA and LV-OOA decreased slightly as a result of the
182 photochemical production. The results here are largely different from our winter study in Handan, a seriously polluted city in
183 Northern China, where primary OA emissions from coal combustion and biomass burning facilitated haze formation (Li et al.,
184 2017b). While in Beijing the contribution of sulfate increased slightly at lower PM_1 concentrations, the sulfate fraction generally
185 presented a mild decrease with elevated PM_1 mass at the two sites. By contrast, nitrate displayed an almost linearly enhanced
186 contribution with increased PM_1 . This observation is consistent with previous summer measurements in Beijing (Sun et al., 2012)
187 and Nanjing (Zhang et al., 2015), China. Accordingly, the nitrate/sulfate mass ratio steadily increased as PM_1 went up.
188 Notably, the large enhancement of nitrate production mainly occurred after midnight. Figure 4 displays the scatter plots of nitrate
189 versus PM_1 as well as sulfate versus PM_1 for comparison, both color-coded by the time of day. Though the ratios of sulfate versus



190 PM₁ mostly increased in the afternoon, nitrate versus PM₁ showed steeper slopes from midnight to early morning. The correlation
191 of nitrate with SV-OOA and LV-OOA also indicated that the formation rate of nitrate is considerably higher than that of SV-OOA
192 and LV-OOA after midnight (Fig. S10). Therefore, we further checked the variations in the mass fractions of aerosol species as a
193 function of PM₁ concentration for two periods, 0:00 to 11:00 and 12:00 to 23:00. Taking Beijing as an example, both the nitrate
194 contribution in PM₁ and the nitrate/sulfate ratio were significantly enhanced for the period of 0:00 to 11:00 (Fig. S11). These results
195 suggest that rapid nitrate formation is mainly associated with nighttime productions, when the heterogeneous hydrolysis of N₂O₅
196 dominates the formation pathways along with higher RH and lower temperature. The observed high N₂O₅ concentrations in urban
197 Beijing further support our hypothesis (Wang et al., 2017). Because the materiality of nitrate formation to haze evolution was
198 observed in both Beijing and Xinxiang, we regard this as the regional generality in summer. Considering the efficient reduction in
199 SO₂ emissions in China (Zhang et al., 2012), the results here highlight the necessity of further NO_x emission control for effective
200 air pollution reduction in Northern China.

201 3.3 Factors influencing the rapid nitrate formation

202 Submicron nitrate mainly exists in the form of semi-volatile ammonium nitrate and is produced by the reaction of NH₃ with HNO₃
203 in the atmosphere. The formation pathways of HNO₃ include the oxidation of NO₂ by OH during the day and the hydrolysis of
204 N₂O₅ at night. Thus, to investigate factors influencing the rapid nitrate formation in summer, the following conditions need to be
205 considered: (1) the abundance of ammonia in the atmosphere, (2) the influence of temperature and RH, and (3) different daytime
206 and nighttime formation mechanisms. Here, we explore nitrate formation processes based on Beijing measurements.

207 Under real atmospheric conditions, NH₃ tends to first react with H₂SO₄ to form (NH₄)₂SO₄ due to its stability (Seinfeld and Pandis,
208 2006). Thus, if possible, each mole of sulfate will remove 2 moles of NH₃ from the gas phase. NH₄NO₃ is formed when excess
209 NH₃ is available. During the sampling period, the observed molar ratios of ammonium to sulfate were mostly larger than 2 (Fig.
210 5), corresponding to an excess of NH₃. The scatter plot of the molar concentration of excess ammonium versus the molar
211 concentration of nitrate showed that, nitrate was completely neutralized by excess ammonium at most times. When ammonium is
212 in deficit, nitrate may associate with other alkaline species or be part of an acidic aerosol.

213 Based on the ISORROPIA-II thermodynamic model, we performed a comprehensive sensitivity analysis of nitrate formation to
214 the gas-phase NH₃ and PM₁ sulfate concentrations. Under typical Beijing summer conditions (T = 300.21K, RH = 56%), we
215 assumed that total inorganic nitrate (HNO₃ + NO₃⁻) in the atmosphere was 10 µg m⁻³. Total ammonia (gas + particle) and PM₁
216 sulfate concentrations were independently varied and input in the ISORROPIA-II model. The predicted equilibrium of the nitrate
217 partitioning ratio ($\epsilon(\text{NO}_3^-) = \text{NO}_3^- / (\text{HNO}_3 + \text{NO}_3^-)$) is shown in Fig. 6. At a sulfate concentration from 0.1 to 45 µg m⁻³, a 10 µg m⁻³
218 increase of gaseous NH₃ generally results in an enhancement of $\epsilon(\text{NO}_3^-)$ by over 0.1 units, thus increasing the particulate nitrate
219 concentration. Interestingly, for ammonia-rich systems, the existence of more particulate sulfate favors the partitioning of nitrate
220 towards the particle phase. The formation of particulate ammonium nitrate is a reversible process with dissociation constant K_p:



222 K_p equals the product of the partial pressures of gaseous NH₃ and HNO₃. For an ammonium sulfate-nitrate solution, K_p not only
223 depends on temperature and RH but also on sulfate concentrations, which is usually expressed by the parameter Y (Seinfeld and
224 Pandis, 2006):

$$225 Y = \frac{[\text{NH}_4\text{NO}_3]}{[\text{NH}_4\text{NO}_3] + 3[(\text{NH}_4)_2\text{SO}_4]} \quad (2)$$

226 When the concentration of ammonium sulfate increases compared to that of ammonium nitrate, the parameter Y decreases and the
227 equilibrium product of NH₃ and HNO₃ decreases. The additional ammonium and sulfate ions make the aqueous system favorable
228 for the formation of ammonium nitrate, by increasing particle liquid water content but not perturbing particle pH significantly.



229 Particle pH is not highly sensitive to sulfate and associated ammonium (Weber et al., 2016; Guo et al., 2017b). Therefore, more
230 ammonium sulfate in the aqueous solution will tend to increase the concentration of ammonium nitrate in the particle phase.
231 However, compared to the significant influence of gaseous NH_3 , $\epsilon(\text{NO}_3^-)$ is weakly sensitive to the sulfate concentration, as shown
232 in Fig. 6. For example, when the ammonia concentration is $10 \mu\text{g m}^{-3}$, a reduction of sulfate from 30 to $20 \mu\text{g m}^{-3}$ has little influence
233 on $\epsilon(\text{NO}_3^-)$. Generally, these results suggest that a decrease in the SO_2 emissions may have a positive effect on nitrate reduction,
234 though controlling NH_3 emissions appears to be more effective.

235 The influence of temperature and RH on nitrate formation was also evaluated based on ISORROPIA-II simulations by varying
236 temperature and RH separately. As shown in Fig. S12, under typical Beijing summer conditions ($T = 30^\circ\text{C}$), $\epsilon(\text{NO}_3^-)$ remains
237 lower than 0.1, even until RH reaches 80%. When $\text{RH} > 90\%$, $\epsilon(\text{NO}_3^-)$ increases sharply as a function of RH. For $T = 0^\circ\text{C}$,
238 representative of Beijing winter conditions, $\epsilon(\text{NO}_3^-)$ is as high as 0.7, even at low RH. Figure 7 demonstrates the variations in the
239 nitrate/sulfate ratio as a function of temperature and RH in Beijing. The nitrate/sulfate ratio increased with decreasing temperature
240 and increasing RH, which drives the nitrate partitioning towards the particle phase. This is further supported by the variations in
241 the equilibrium constant K_{AN} of Eq. (1), which can be calculated as:

$$242 K_{\text{AN}} = K_{\text{AN}}(298 \text{ K}) \exp \left\{ a \left(\frac{298}{T} - 1 \right) + b \left[1 + \ln \left(\frac{298}{T} \right) - \frac{298}{T} \right] \right\} \quad (3)$$

243 where T is the ambient temperature in Kelvin, $K_{\text{AN}}(298) = 3.36 \times 10^{16} (\text{atm}^{-2})$, $a = 75.11$, and $b = -13.5$ (Seinfeld and Pandis, 2006).
244 Similar to the nitrate/sulfate ratio, the diurnal profile of K_{AN} peaks at night due to the lower temperature and higher RH.

245 As described in Sect. 3.2, the rapid nitrate formation in this study appeared to be mainly associated with its nighttime enhancement.
246 In addition to the effects of temperature and RH, the nighttime nitrate formation pathways may also play a role. Overnight,
247 particulate nitrate primarily forms via the heterogeneous hydrolysis of N_2O_5 on the wet surface of aerosol (Ravishankara, 1997).
248 N_2O_5 is produced by the reversible reaction between NO_2 and the NO_3 radical, where NO_2 reacts with O_3 to form the NO_3 radical.
249 Assuming N_2O_5 and the NO_3 radical are both in steady state considering their short lifetimes (Brown et al., 2006), the nighttime
250 production of N_2O_5 and HNO_3 is proportional to the concentration of NO_2 and O_3 ($[\text{NO}_2][\text{O}_3]$) (Young et al., 2016; Kim et al.,
251 2017). For the different PM_1 concentration bins, we examined the NO_2 and O_3 data at 0:00 to assess the nighttime HNO_3 production
252 rate. It can be seen that $[\text{NO}_2][\text{O}_3]$ was obviously enhanced with an increase in the PM_1 mass loading (Fig. S13), implying that
253 nitrate formation by the N_2O_5 pathway favors the driving role of nitrate in haze evolution.

254 According to the Multi-resolution Emission Inventory for China (MEIC, <http://www.meicmodel.org>), NO_x emissions localized in
255 Beijing are much smaller than emissions in adjacent Hebei, Shandong, and Henan provinces. In Fig. 1, episodes in Beijing,
256 characterized by largely enhanced nitrate concentrations, usually occurred with the change in the wind direction from north and
257 west to south and east, where the highly polluted Hebei, Shandong, and Henan provinces are located. When the relatively clean air
258 masses from north and west returned, aerosol pollution was instantly swept away. Therefore, the importance of regional transport
259 on haze formation in Beijing should also be considered. We examined the association of aerosol concentration and composition
260 with air mass origins determined through cluster analysis of HYSPLIT back trajectories. As illustrated in Fig. 8, the aerosol
261 characteristics are quite different for air masses from different regions. Cluster 1 mainly passed through Shanxi and Hebei provinces,
262 and Cluster 2 originated from Hebei, Shandong, and Henan provinces. Consistent with the high air pollutant emissions in these
263 areas, Cluster 1 and Cluster 2 were characterized with high PM_1 concentrations and high contributions of secondary aerosols. The
264 nitrate fraction in PM_1 was 24% for Cluster 1 and 26% for Cluster 2. In comparison, Cluster 3 and Cluster 4 resulted from long-
265 range transport from the cleaner northern areas and were correspondingly characterized by lower PM_1 concentrations. Organics
266 dominated PM_1 for Cluster 3 and Cluster 4, with a nitrate contribution of 14% and 16%, respectively. Figure S14 shows the cluster
267 distribution as a function of PM_1 concentration. With an increase in the PM_1 mass, the contribution of cleaner Cluster 3 and Cluster



268 4 significantly decreased. When PM_1 concentrations were above $20 \mu g m^{-3}$, the air masses arriving in Beijing were mostly
269 contributed by Cluster 1 and Cluster 2, which led to rapid nitrate accumulation.

270 3.4 Comparison with other regions and policy implications

271 Figure 9 summarizes the chemical composition of PM_1 or NR- PM_1 (BC excluded) measured during the summer in Asia, Europe,
272 and North America. Three types of sampling locations were included: urban areas, urban downwind areas, and rural/remote areas.
273 Aerosol particles were dominated by organics (25.5-80.4%; avg = 48.1%) and secondary inorganic aerosols (18.0-73.7%; avg =
274 47.3%), and the nitrate contribution largely varied among different locations. Data for the pie charts are given in Table S3.
275 For further comparison, we classified the datasets into three groups according to the location type and examined their difference
276 in nitrate mass concentrations and mass contributions. Overall, the nitrate concentrations varied from $0.04 \mu g m^{-3}$ to $17.6 \mu g m^{-3}$ in
277 summer, with contributions of 0.9% to 25.2%. Patterns in Fig. 10 demonstrate that the nitrate concentrations in mainland China
278 are usually much higher than those in other areas, consistent with the severe haze pollution in China. In particular, the percentage
279 of nitrate in aerosol particles is generally several times higher in mainland China than in other regions, except for measurements
280 in Riverside, CA, which were conducted near the local highway (Docherty et al., 2011). Compared to rural/remote areas, nitrate
281 shows higher mass concentrations and mass fractions in urban and urban downwind areas, revealing the influence of anthropogenic
282 emissions, i.e., traffic and power plant, on nitrate formation. In Beijing, the capital of China, field measurements among different
283 years show an obvious reduction in the nitrate mass concentration, especially from 2012. This coincides with the decline in satellite-
284 observed NO_2 levels in China after 2011 (Miyazaki et al., 2017) and a 21% decrease in NO_x emissions from 2011 to 2015 based
285 on a bottom-up emission inventory (Liu et al., 2017). Detailed analysis by Liu et al. (2017) revealed that the NO_x decline in China
286 in recent years is mainly driven by the penetration of selective catalytic reduction (SCR) in power plants and strict regulations for
287 vehicle emissions. The large decrease in nitrate concentration in the summer of 2008 was primarily caused by the strict emission
288 control measures implemented during the 2008 Olympic Games (Wang et al., 2010). However, nitrate contributions in China still
289 remain high over the years, especially in urban and urban downwind areas, indicating the importance of nitrate formation in haze
290 episodes. Overall, the higher concentration and, in particular, the higher contribution of nitrate in aerosol particles during
291 summertime call for the urgent need of further NO_x reduction measures and NH_3 emission control in China.

292 4 Conclusions

293 Summertime field measurements were conducted in both Beijing (30 June to 27 July, 2015) and Xinxiang (8 to 25 June, 2017) in
294 the NCP region, using state-of-the-art online instruments to investigate the factors driving aerosol pollution. The average PM_1
295 concentration was $35.0 \mu g m^{-3}$ in Beijing and $64.2 \mu g m^{-3}$ in Xinxiang, with the hourly maximum reaching $114.9 \mu g m^{-3}$ and 208.1
296 $\mu g m^{-3}$, respectively. Pollution episodes along with significantly enhanced nitrate concentrations were frequently observed during
297 the campaigns. Secondary inorganic aerosol dominated the PM_1 mass, with higher nitrate contributions of 24% in Beijing and 26%
298 in Xinxiang. The diurnal profile of nitrate presented higher concentrations at night and lower values in the afternoon. By eliminating
299 the influences of different dilution/mixing conditions due to boundary layer development, we found that the lower nitrate
300 concentrations in the afternoon were caused by the strong evaporative loss of nitrate at higher temperatures, which overcame the
301 daytime photochemical production of nitrate. With the development of aerosol pollution, OA showed a decreasing contribution to
302 total PM_1 , despite its obvious domination at lower PM_1 mass loadings. The reduction in the OA mass fraction was primarily driven
303 by primary sources, especially in Beijing. Generally, the mass fraction of sulfate also decreased slightly as a function of PM_1
304 concentration. In contrast, nitrate presented an almost linearly enhanced contribution with the elevation of PM_1 mass, suggesting



305 the important role of nitrate formation in causing high aerosol pollution during summer. Rapid nitrate production mainly occurred
306 after midnight, and the formation rate was higher for nitrate than for sulfate, SV-OOA, or LV-OOA.
307 Comprehensive analysis of nitrate behaviors revealed that abundant ammonia emissions in the NCP region favored nitrate
308 production in summer. According to the ISORROPIA-II thermodynamic predictions, $\varepsilon(\text{NO}_3^-)$ is significantly increased when there
309 is more gas-phase ammonia in the atmosphere. Decreased SO_2 emissions may have co-beneficial impacts on nitrate reduction.
310 Lower temperature and higher RH shift the equilibrium partitioning of nitrate towards the particle phase, thus increasing the
311 particulate nitrate concentration. Assuming both N_2O_5 and NO_3 radicals are in steady state, $[\text{NO}_2][\text{O}_3]$ can be used as an indicator
312 to evaluate the contribution of nighttime N_2O_5 hydrolysis to nitrate formation. With the anabatic pollution levels, $[\text{NO}_2][\text{O}_3]$
313 obviously enhanced at night along with higher RH, suggesting the increased role of nighttime nitrate production in haze evolution.
314 Based on cluster analysis via the HYSPLIT model, nitrate formation was also found to depend on regional transport from different
315 air mass origins, in accordance with the spatial distribution of NO_x emissions in the NCP region.
316 Finally, nitrate data acquired from this study were integrated with the literature results, including various field measurements
317 conducted in Asia, Europe, and North America. Nitrate is present in higher mass concentrations and mass fractions in China than
318 in other regions. Due to the large anthropogenic emissions in urban and urban downwind areas, the mass concentrations and mass
319 contributions of nitrate are much higher in these regions than in remote/rural areas. Although the nitrate mass concentrations in
320 Beijing have steadily decreased over the years, its contribution still remains high, emphasizing the significance of further NO_x
321 reduction and the initiation of NH_3 emission control in China.
322 Most of the previous studies conducted during wintertime reveal that secondary formation of sulfate together with primary
323 emissions from coal combustion and biomass burning are important driving factors of haze evolution in the NCP region. According
324 to this study, in Beijing and Xinxiang, rapid nitrate formation is regarded as the propulsion of aerosol pollution during summertime.
325 Therefore, to better balance economic development and air pollution control, different emission control measures could be
326 established corresponding to the specific driving forces of air pollution in different seasons. Further studies on seasonal variations
327 are needed to test the conclusions presented here and provide more information on haze evolution in spring and fall.

328 Acknowledgements

329 This work was funded by the National Natural Science Foundation of China (41571130035, 41571130032 and 41625020).

330 References

331 Alexander, B., Hastings, M. G., Allman, D. J., Dachs, J., Thornton, J. A., and Kunasek, S. A.: Quantifying atmospheric nitrate
332 formation pathways based on a global model of the oxygen isotopic composition (17O) of atmospheric nitrate, *Atmos. Chem.
333 Phys.*, 9, 5043–5056, doi:10.5194/acp-9-5043-2009, 2009.
334 Bougiatioti, A., Nikolaou, P., Stavroulas, I., Kouvarakis, G., Weber, R., Nenes, A., Kanakidou, M., and Mihalopoulos, N.: Particle
335 water and pH in the eastern Mediterranean: source variability and implications for nutrient availability, *Atmos. Chem. Phys.*,
336 16, 4579–4591, 10.5194/acp-16-4579-2016, 2016.
337 Brown, S. S., Ryerson, T. B., Wollny, A. G., Brock, C. A., Peltier, R., Sullivan, A. P., Weber, R. J., Dube, W. P., Trainer, M.,
338 Meagher, J. F., Fehsenfeld, F. C., and Ravishankara, A. R.: Variability in nocturnal nitrogen oxide processing and its role in
339 regional air quality, *Science*, 311, 67–70, 10.1126/science.1120120, 2006.
340 Cheng, Y. F., Zheng, G. J., Wei, C., Mu, Q., Zheng, B., Wang, Z. B., Gao, M., Zhang, Q., He, K. B., Carmichael, G., Poschl, U.,
341 and Su, H.: Reactive nitrogen chemistry in aerosol water as a source of sulfate during haze events in China, *Science Advances*,
342 2, ARTN e1601530 10.1126/sciadv.1601530, 2016.
343 Cohen, A. J., Brauer, M., Burnett, R., Anderson, H. R., Frostad, J., Estep, K., Balakrishnan, K., Brunekreef, B., Dandona, L.,
344 Dandona, R., Feigin, V., Freedman, G., Hubbell, B., Jobling, A., Kan, H., Knibbs, L., Liu, Y., Martin, R., Morawska, L., Pope,
345 C. A., Shin, H., Straif, K., Shaddick, G., Thomas, M., van Dingenen, R., van Donkelaar, A., Vos, T., Murray, C. J. L., and
346 Forouzanfar, M. H.: Estimates and 25-year trends of the global burden of disease attributable to ambient air pollution: an



347 analysis of data from the Global Burden of Diseases Study 2015, *Lancet*, 389, 1907-1918, 10.1016/S0140-6736(17)30505-6,
348 2017.

349 Docherty, K. S., Aiken, A. C., Huffman, J. A., Ulbrich, I. M., DeCarlo, P. F., Sueper, D., Worsnop, D. R., Snyder, D. C., Peltier,
350 R. E., Weber, R. J., Grover, B. D., Eatough, D. J., Williams, B. J., Goldstein, A. H., Ziemann, P. J., and Jimenez, J. L.: The
351 2005 Study of Organic Aerosols at Riverside (SOAR-1): instrumental intercomparisons and fine particle composition, *Atmos.*
352 *Chem. Phys.*, 11, 12387-12420, <https://doi.org/10.5194/acp-11-12387-2011>, 2011.

353 Draxier, R. R., and Hess, G. D.: An overview of the HYSPLIT_4 modelling system for trajectories, dispersion and deposition,
354 *Aust Meteorol Mag*, 47, 295-308, 1998.

355 Fountoukis, C. and Nenes, A.: ISORROPIA II: a computationally efficient thermodynamic equilibrium model for $K^+ - Ca^{2+} - Mg^{2+} -$
356 $NH_4^+ - Na^+ - SO_4^{2-} - NO_3^- - Cl^- - H_2O$ aerosols, *Atmos. Chem. Phys.*, 7, 4639-4659, <https://doi.org/10.5194/acp-7-4639-2007>,
357 2007.

358 Guo, H., Xu, L., Bougiatioti, A., Cerully, K. M., Capps, S. L., Hite, J. R., Carlton, A. G., Lee, S. H., Bergin, M. H., Ng, N. L.,
359 Nenes, A., and Weber, R. J.: Fine-particle water and pH in the southeastern United States, *Atmos Chem Phys*, 15, 5211-5228,
360 10.5194/acp-15-5211-2015, 2015.

361 Guo, H., Sullivan, A. P., Campuzano-Jost, P., Schroder, J. C., Lopez-Hilfiker, F. D., Dibb, J. E., Jimenez, J. L., Thornton, J. A.,
362 Brown, S. S., Nenes, A., and Weber, R. J.: Fine particle pH and the partitioning of nitric acid during winter in the northeastern
363 United States, *J Geophys Res-Atmos*, 121, 10355-10376, 10.1002/2016JD025311, 2016.

364 Guo, H. Y., Liu, J. M., Froyd, K. D., Roberts, J. M., Veres, P. R., Hayes, P. L., Jimenez, J. L., Nenes, A., and Weber, R. J.: Fine
365 particle pH and gas-particle phase partitioning of inorganic species in Pasadena, California, during the 2010 CalNex campaign,
366 *Atmos Chem Phys*, 17, 5703-5719, 10.5194/acp-17-5703-2017, 2017a.

367 Guo, H. Y., Weber, R. J., and Nenes, A.: High levels of ammonia do not raise fine particle pH sufficiently to yield nitrogen oxide-
368 dominated sulfate production, *Sci Rep-Uk*, 7, Artn 12109 10.1038/S41598-017-11704-0, 2017b.

369 Guo, S., Hu, M., Zamora, M. L., Peng, J. F., Shang, D. J., Zheng, J., Du, Z. F., Wu, Z., Shao, M., Zeng, L. M., Molina, M. J., and
370 Zhang, R. Y.: Elucidating severe urban haze formation in China, *P Natl Acad Sci USA*, 111, 17373-17378,
371 10.1073/pnas.1419604111, 2014.

372 Hennigan, C. J., Izumi, J., Sullivan, A. P., Weber, R. J., and Nenes, A.: A critical evaluation of proxy methods used to estimate the
373 acidity of atmospheric particles, *Atmos Chem Phys*, 15, 2775-2790, 10.5194/acp-15-2775-2015, 2015.

374 Hu, W., Hu, M., Hu, W. W., Zheng, J., Chen, C., Wu, Y. S., and Guo, S.: Seasonal variations in high time-resolved chemical
375 compositions, sources, and evolution of atmospheric submicron aerosols in the megacity Beijing, *Atmos Chem Phys*, 17,
376 9979-10000, 10.5194/acp-17-9979-2017, 2017.

377 Hu, W. W., Hu, M., Hu, W., Jimenez, J. L., Yuan, B., Chen, W. T., Wang, M., Wu, Y. S., Chen, C., Wang, Z. B., Peng, J. F., Zeng,
378 L. M., and Shao, M.: Chemical composition, sources, and aging process of submicron aerosols in Beijing: Contrast between
379 summer and winter, *J Geophys Res-Atmos*, 121, 1955-1977, 10.1002/2015JD024020, 2016.

380 Huang, R. J., Zhang, Y. L., Bozzetti, C., Ho, K. F., Cao, J. J., Han, Y. M., Daelenbach, K. R., Slowik, J. G., Platt, S. M., Canonaco,
381 F., Zotter, P., Wolf, R., Pieber, S. M., Bruns, E. A., Crippa, M., Ciarelli, G., Piazzalunga, A., Schwikowski, M., Abbaszade,
382 G., Schnelle-Kreis, J., Zimmermann, R., An, Z. S., Szidat, S., Baltensperger, U., El Haddad, I., and Prevot, A. S. H.: High
383 secondary aerosol contribution to particulate pollution during haze events in China, *Nature*, 514, 218-222,
384 10.1038/nature13774, 2014.

385 IPCC: Summary for Policymakers, in: *Climate Change 2007: The Physical Science Basis. Contribution of Working Group I to the*
386 *Fourth Assessment Report of the Intergovernmental Panel on Climate Change*, edited by: Solomon, S., Qin, D., Manning, M.,
387 Chen, Z., Marquis, M., Averyt, K. B., Tignor, M., and Miller, H. L., Cambridge University Press, Cambridge, UK and New
388 York, NY, USA, 1-18, 2007.

389 Jimenez, J. L., Canagaratna, M. R., Donahue, N. M., Prevot, A. S. H., Zhang, Q., Kroll, J. H., DeCarlo, P. F., Allan, J. D., Coe, H.,
390 Ng, N. L., Aiken, A. C., Docherty, K. S., Ulbrich, I. M., Grieshop, A. P., Robinson, A. L., Duplissy, J., Smith, J. D., Wilson,
391 K. R., Lanz, V. A., Hueglin, C., Sun, Y. L., Tian, J., Laaksonen, A., Raatikainen, T., Rautiainen, J., Vaattovaara, P., Ehn, M.,
392 Kulmala, M., Tomlinson, J. M., Collins, D. R., Cubison, M. J., Dunlea, E. J., Huffman, J. A., Onasch, T. B., Alfarra, M. R.,
393 Williams, P. I., Bower, K., Kondo, Y., Schneider, J., Drewnick, F., Borrmann, S., Weimer, S., Demerjian, K., Salcedo, D.,
394 Cottrell, L., Griffin, R., Takami, A., Miyoshi, T., Hatakeyama, S., Shimono, A., Sun, J. Y., Zhang, Y. M., Dzepina, K.,
395 Kimmel, J. R., Sueper, D., Jayne, J. T., Herndon, S. C., Trimborn, A. M., Williams, L. R., Wood, E. C., Middlebrook, A. M.,
396 Kolb, C. E., Baltensperger, U., and Worsnop, D. R.: Evolution of Organic Aerosols in the Atmosphere, *Science*, 326, 1525-
397 1529, 10.1126/science.1180353, 2009.

398 Kim, H., Zhang, Q., and Heo, J.: Influence of Intense secondary aerosol formation and long range transport on aerosol chemistry
399 and properties in the Seoul Metropolitan Area during spring time: Results from KORUS-AQ, *Atmos. Chem. Phys. Discuss.*,
400 <https://doi.org/10.5194/acp-2017-947>, in review, 2017.

401 Li, H., Zhang, Q., Duan, F., Zheng, B., and He, K.: The “Parade Blue”: effects of short-term emission control on aerosol chemistry,
402 *Faraday Discuss.*, 189, 317-335, 2016.

403 Li, Y. J., Sun, Y., Zhang, Q., Li, X., Li, M., Zhou, Z., and Chan, C. K.: Real-time chemical characterization of atmospheric
404 particulate matter in China: A review, *Atmos Environ*, 158, 270-304, <https://doi.org/10.1016/j.atmosenv.2017.02.027>, 2017a.

405 Li, H. Y., Zhang, Q., Zhang, Q., Chen, C. R., Wang, L. T., Wei, Z., Zhou, S., Parworth, C., Zheng, B., Canonaco, F., Prevot, A. S.
406 H., Chen, P., Zhang, H. L., Wallington, T. J., and He, K. B.: Wintertime aerosol chemistry and haze evolution in an extremely



407 polluted city of the North China Plain: significant contribution from coal and biomass combustion, *Atmos. Chem. Phys.*, 17,
408 4751-4768, 10.5194/acp-17-4751-2017, 2017b.

409 Li, C., McLinden, C., Fioletov, V., Krotkov, N., Carn, S., Joiner, J., Streets, D., He, H., Ren, X. R., Li, Z. Q., and Dickerson, R.
410 R.: India Is Overtaking China as the World's Largest Emitter of Anthropogenic Sulfur Dioxide, *Sci. Rep.-Uk.*, 7, Artn 14304
411 10.1038/S41598-017-14639-8, 2017c.

412 Liu, F., Beirle, S., Zhang, Q., van der A, R. J., Zheng, B., Tong, D., and He, K. B.: NO_x emission trends over Chinese cities
413 estimated from OMI observations during 2005 to 2015, *Atmos. Chem. Phys.*, 17, 9261-9275, 10.5194/acp-17-9261-2017, 2017.

414 Liu, M., Song, Y., Zhou, T., Xu, Z., Yan, C., Zheng, M., Wu, Z., Hu, M., Wu, Y., and Zhu, T.: Fine particle pH during severe haze
415 episodes in northern China, *Geophys. Res. Lett.*, 44, 2017GL073210, 10.1002/2017GL073210, 2017.

416 Miyazaki, K., Eskes, H., Sudo, K., Boersma, K. F., Bowman, K., and Kanaya, Y.: Decadal changes in global surface NO_x emissions
417 from multi-constituent satellite data assimilation, *Atmos. Chem. Phys.*, 17, 807-837, <https://doi.org/10.5194/acp-17-807-2017>,
418 2017.

419 Ng, N. L., Herndon, S. C., Trimborn, A., Canagaratna, M. R., Croteau, P. L., Onasch, T. B., Sueper, D., Worsnop, D. R., Zhang,
420 Q., Sun, Y. L., and Jayne, J. T.: An Aerosol Chemical Speciation Monitor (ACSM) for Routine Monitoring of the Composition
421 and Mass Concentrations of Ambient Aerosol, *Aerosol Sci. Tech.*, 45, 780-794, Pii 934555189
422 10.1080/02786826.2011.560211, 2011.

423 Paatero, P., and Tapper, U.: Positive Matrix Factorization - a Nonnegative Factor Model with Optimal Utilization of Error-
424 Estimates of Data Values, *Environmetrics*, 5, 111-126, DOI 10.1002/env.3170050203, 1994.

425 Pathak, R. K., Wang, T., and Wu, W. S.: Nighttime enhancement of PM2.5 nitrate in ammonia-poor atmospheric conditions in
426 Beijing and Shanghai: Plausible contributions of heterogeneous hydrolysis of N₂O₅ and HNO₃ partitioning, *Atmos. Environ.*,
427 45, 1183-1191, 10.1016/j.atmosenv.2010.09.003, 2011.

428 Petzold, A. and Schonlinner, M.: Multi-angle absorption photometry – a new method for the measurement of aerosol light
429 absorption and atmospheric black carbon, *J. Aerosol Sci.*, 35, 421–441, 2004.

430 Petzold, A., Schloesser, H., Sheridan, P. J., Arnott, W. P., Ogren, J. A., and Virkkula, A.: Evaluation of multiangle absorption
431 photometry for measuring aerosol light absorption, *Aerosol Sci. Tech.*, 39, 40–51, 2005.

432 Pope, C. A., Ezzati, M., and Dockery, D. W.: Fine-Particulate Air Pollution and Life Expectancy in the United States, *New England
433 Journal of Medicine*, 360, 376–386, doi:10.1056/NEJMsa0805646, 2009.

434 Ravishankara, A. R.: Heterogeneous and multiphase chemistry in the troposphere, *Science*, 276, 1058-1065, DOI
435 10.1126/science.276.5315.1058, 1997.

436 Seinfeld, J. H. and Pandis, S. N.: *Atmospheric Chemistry and Physics: From Air Pollution to Climate Change*, John Wiley & Sons,
437 New York, 2nd edition, 1232 pp., ISBN-13: 978-0-471-72018-8, 2006.

438 Sun, Y. L., Wang, Z. F., Dong, H. B., Yang, T., Li, J., Pan, X. L., Chen, P., and Jayne, J. T.: Characterization of summer organic
439 and inorganic aerosols in Beijing, China with an Aerosol Chemical Speciation Monitor, *Atmos. Environ.*, 51, 250-259,
440 10.1016/j.atmosenv.2012.01.013, 2012.

441 Sun, Y. L., Wang, Z. F., Dong, H. B., Yang, T., Li, J., Pan, X. L., Chen, P., and Jayne, J. T.: Characterization of summer organic
442 and inorganic aerosols in Beijing, China with an Aerosol Chemical Speciation Monitor, *Atmos. Environ.*, 51, 250-259,
443 10.1016/j.atmosenv.2012.01.013, 2012. Sun, Y. L., Wang, Z. F., Du, W., Zhang, Q., Wang, Q. Q., Fu, P. Q., Pan, X. L., Li,
444 J., Jayne, J., and Worsnop, D. R.: Long-term real-time measurements of aerosol particle composition in Beijing, China: seasonal
445 variations, meteorological effects, and source analysis, *Atmos. Chem. Phys.*, 15, 10149-10165, 10.5194/acp-15-10149-
446 2015, 2015.

447 Ulbrich, I. M., Canagaratna, M. R., Zhang, Q., Worsnop, D. R., and Jimenez, J. L.: Interpretation of organic components from
448 Positive Matrix Factorization of aerosol mass spectrometric data, *Atmos. Chem. Phys.*, 9, 2891-2918, 10.5194/acp-9-2891-
449 2009, 2009.

450 Watson, J. G.: Visibility: Science and regulation, *J. Air Waste Manage. Assoc.*, 52, 628–713,
451 doi:10.1080/10473289.2002.10470813, 2002.

452 Wang, H., Lu, K., Chen, X., Zhu, Q., Chen, Q., Guo, S., Jiang, M., Li, X., Shang, D., Tan, Z., Wu, Y., Wu, Z., Zou, Q., Zheng, Y.,
453 Zeng, L., Zhu, T., Hu, M., and Zhang, Y.: High N₂O₅ Concentrations Observed in Urban Beijing: Implications of a Large
454 Nitrate Formation Pathway, *Environ. Sci. Tech. Lett.*, 10.1021/acs.estlett.7b00341, 2017.

455 Wang, S. X., Zhao, M., Xing, J., Wu, Y., Zhou, Y., Lei, Y., He, K. B., Fu, L. X., and Hao, J. M.: Quantifying the Air Pollutants
456 Emission Reduction during the 2008 Olympic Games in Beijing, *Environ. Sci. Technol.*, 44, 2490-2496, 10.1021/es9028167,
457 2010.

458 Weber, R. J., Guo, H. Y., Russell, A. G., and Nenes, A.: High aerosol acidity despite declining atmospheric sulfate concentrations
459 over the past 15 years, *Nat. Geosci.*, 9, 282–+, 10.1038/NGEO2665, 2016.

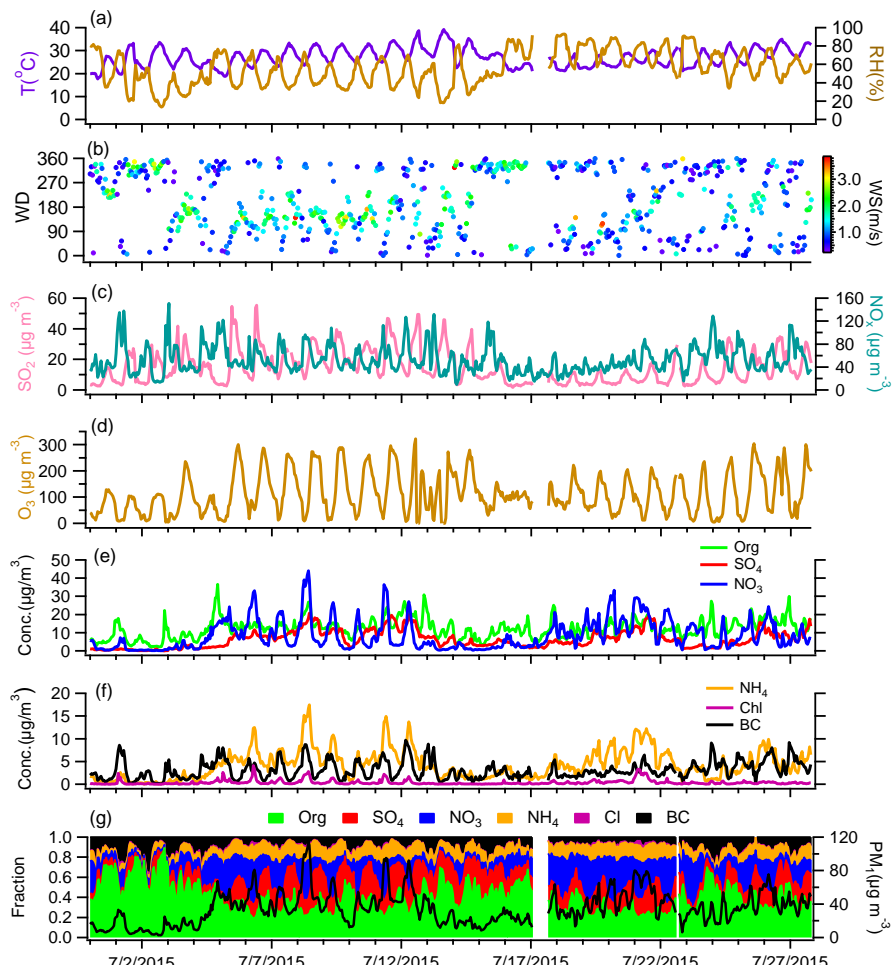
460 Yang, T., Sun, Y., Zhang, W., Wang, Z., Liu, X., Fu, P., and Wang, X.: Evolutionary processes and sources of high-nitrate haze
461 episodes over Beijing, Spring, *J. Environ. Sci.-China*, 54, 142-151, <http://dx.doi.org/10.1016/j.jes.2016.04.024>, 2017.

462 Young, D. E., Kim, H., Parworth, C., Zhou, S., Zhang, X. L., Cappa, C. D., Seco, R., Kim, S., and Zhang, Q.: Influences of emission
463 sources and meteorology on aerosol chemistry in a polluted urban environment: results from DISCOVER-AQ California,
464 *Atmos. Chem. Phys.*, 16, 5427-5451, 10.5194/acp-16-5427-2016, 2016.

465 Zhang, Q., Jimenez, J. L., Canagaratna, M. R., Ulbrich, I. M., Ng, N. L., Worsnop, D. R., and Sun, Y.: Understanding atmospheric
466 organic aerosols via factor analysis of aerosol mass spectrometry: a review, *Anal. Bioanal. Chem.*, 401, 3045–3067, 2011.

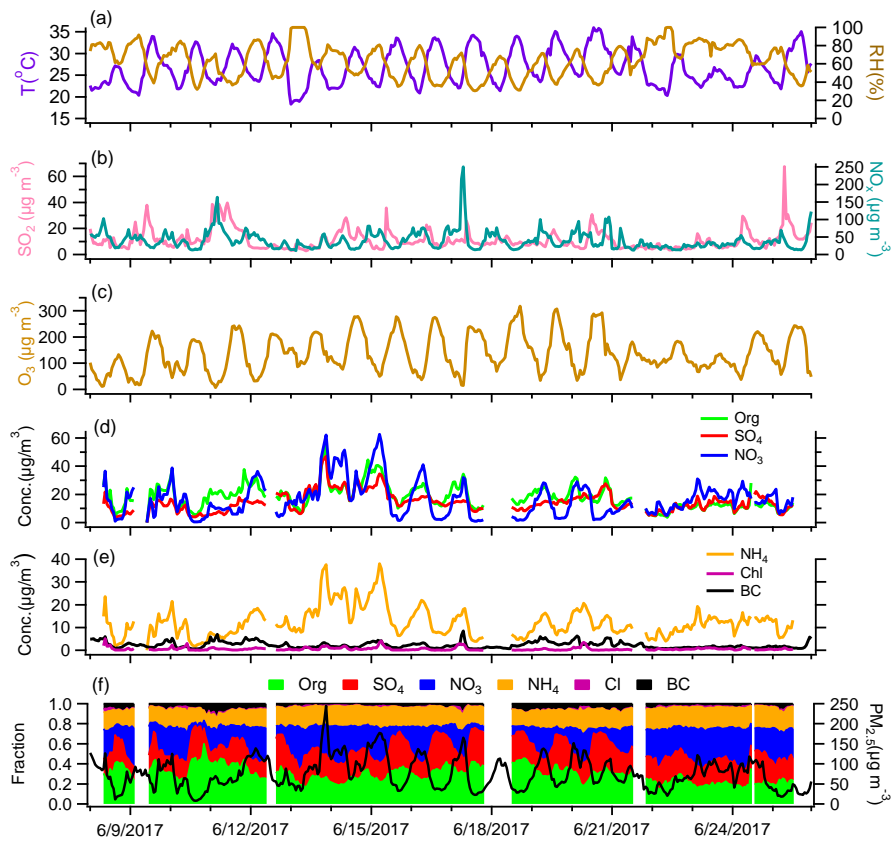


467 Zhang, Q., He, K. B., and Huo, H.: Cleaning China's air, *Nature*, 484, 161-162, 2012.
468 Zhang, Y. J., Tang, L. L., Wang, Z., Yu, H. X., Sun, Y. L., Liu, D., Qin, W., Canonaco, F., Prevot, A. S. H., Zhang, H. L., and
469 Zhou, H. C.: Insights into characteristics, sources, and evolution of submicron aerosols during harvest seasons in the Yangtze
470 River delta region, China, *Atmos Chem Phys*, 15, 1331-1349, 10.5194/acp-15-1331-2015, 2015.
471 Zheng, B., Zhang, Q., Zhang, Y., He, K. B., Wang, K., Zheng, G. J., Duan, F. K., Ma, Y. L., and Kimoto, T.: Heterogeneous
472 chemistry: a mechanism missing in current models to explain secondary inorganic aerosol formation during the January 2013
473 haze episode in North China, *Atmos Chem Phys*, 15, 2031-2049, 10.5194/acp-15-2031-2015, 2015.
474 Zou, Y., Wang, Y., Zhang, Y., and Koo, J.-H.: Arctic sea ice, Eurasia snow, and extreme winter haze in China, *Science Advances*,
475 3, 10.1126/sciadv.1602751, 2017.
476



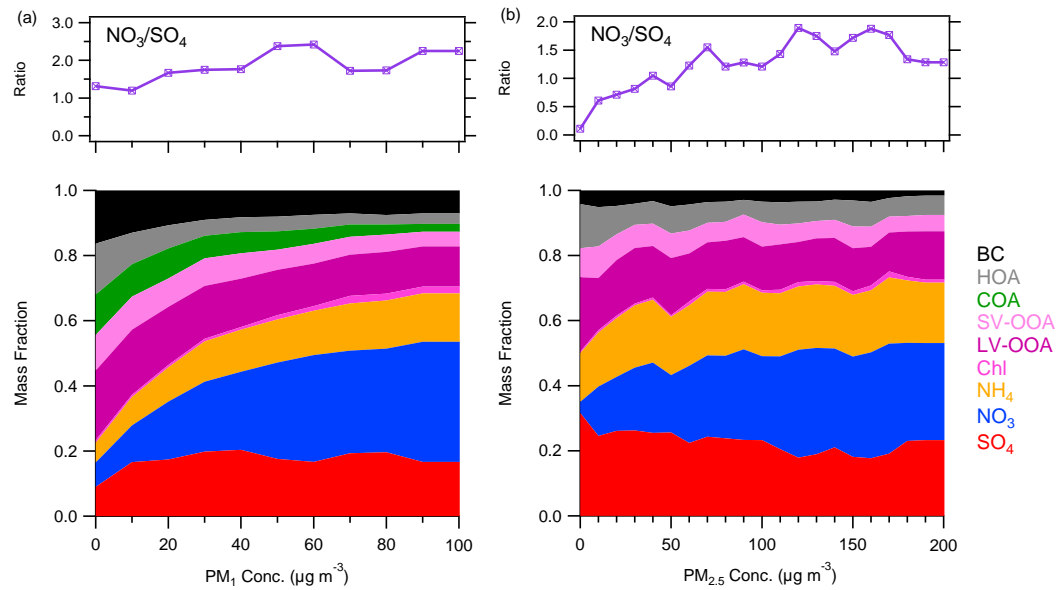
477
478 **Figure 1.** Time series of meteorological parameters, gaseous species, and submicron aerosol species in Beijing.

479



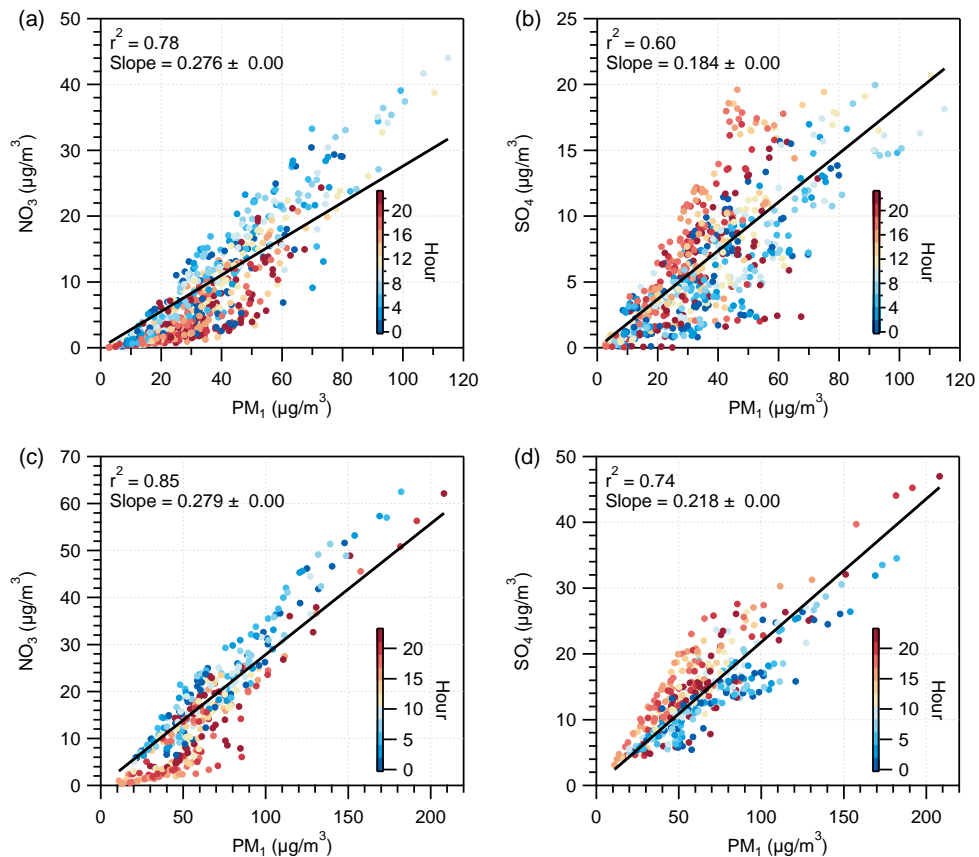
480

481 Figure 2. Time series of meteorological parameters, gaseous species, and submicron aerosol species in Xinxiang.



482

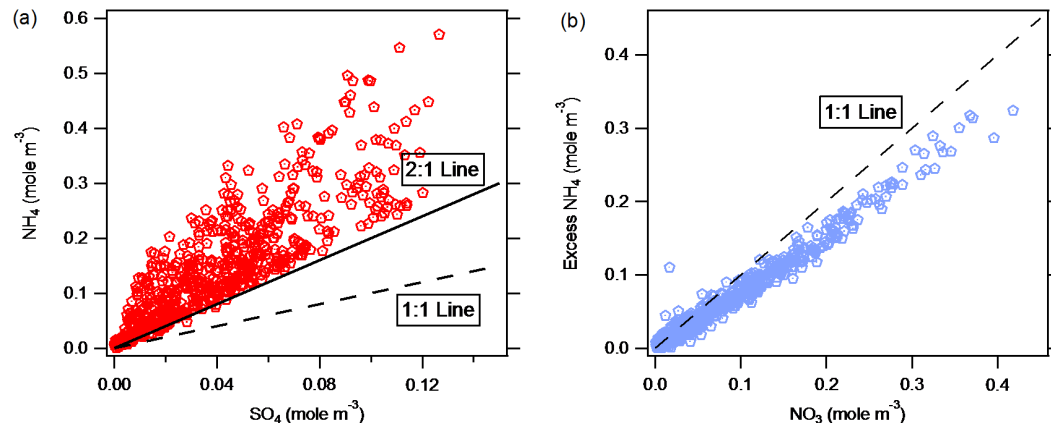
483 **Figure 3. Variations in the mass fraction of aerosol species and nitrate/sulfate mass ratio as a function of total PM_1 mass loadings in (a)**
484 **Beijing and (b) Xinxiang.**



485

486 **Figure 4.** Scatterplots of nitrate vs. PM₁ concentration and sulfate vs. PM₁ concentration, colored by the hour of the day, in (a-b) Beijing
487 and (c-d) Xinxiang.

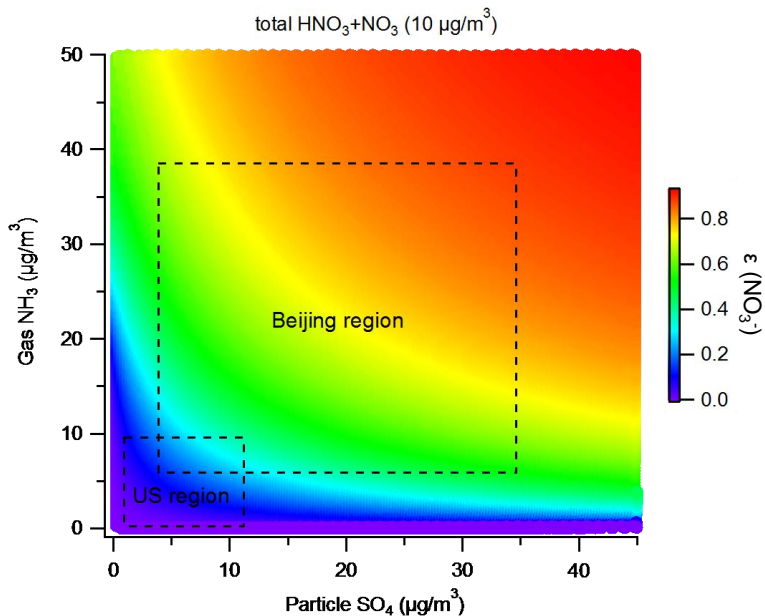
488



489

490 **Figure 5.** Comparison of the molar concentrations of (a) ammonium and sulfate (the 2:1 reference line represents complete H_2SO_4
491 neutralization) and (b) excess ammonium and nitrate (the 1:1 reference line represents complete HNO_3 neutralization).

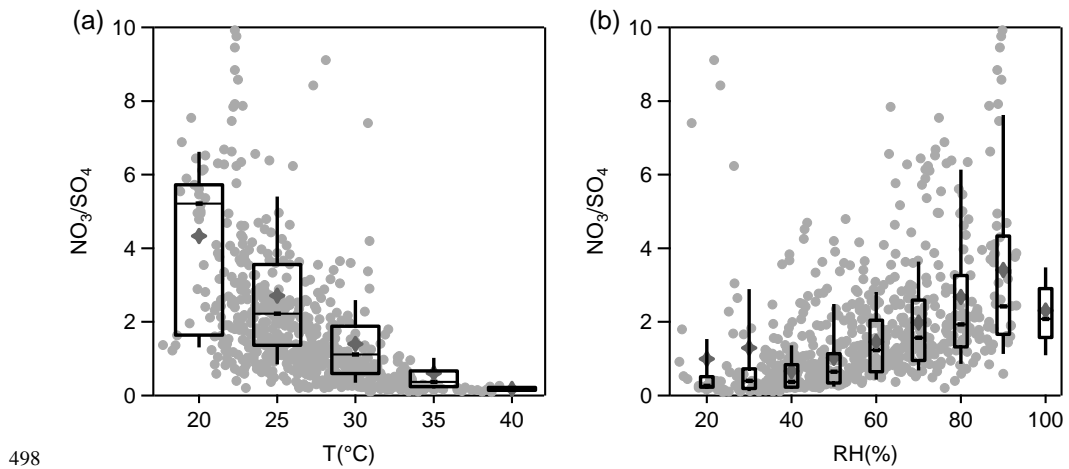
492



493

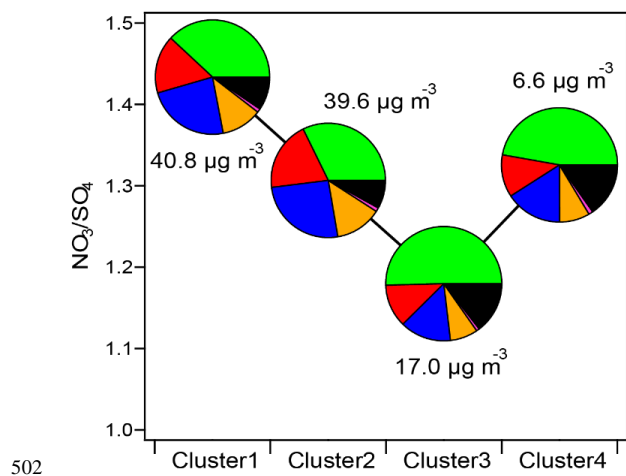
494 Figure 6. Sensitivity of the nitrate partitioning ratio ($\epsilon(\text{NO}_3) = \text{NO}_3^+ / (\text{HNO}_3 + \text{NO}_3^+)$) to gas-phase ammonia and PM_1 sulfate
495 concentrations based on thermodynamic predictions under typical Beijing and Xinxiang summertime conditions. The total nitrate
496 concentration is assumed to be 10 $\mu\text{g m}^{-3}$, according to the observed PM_1 nitrate concentration.

497

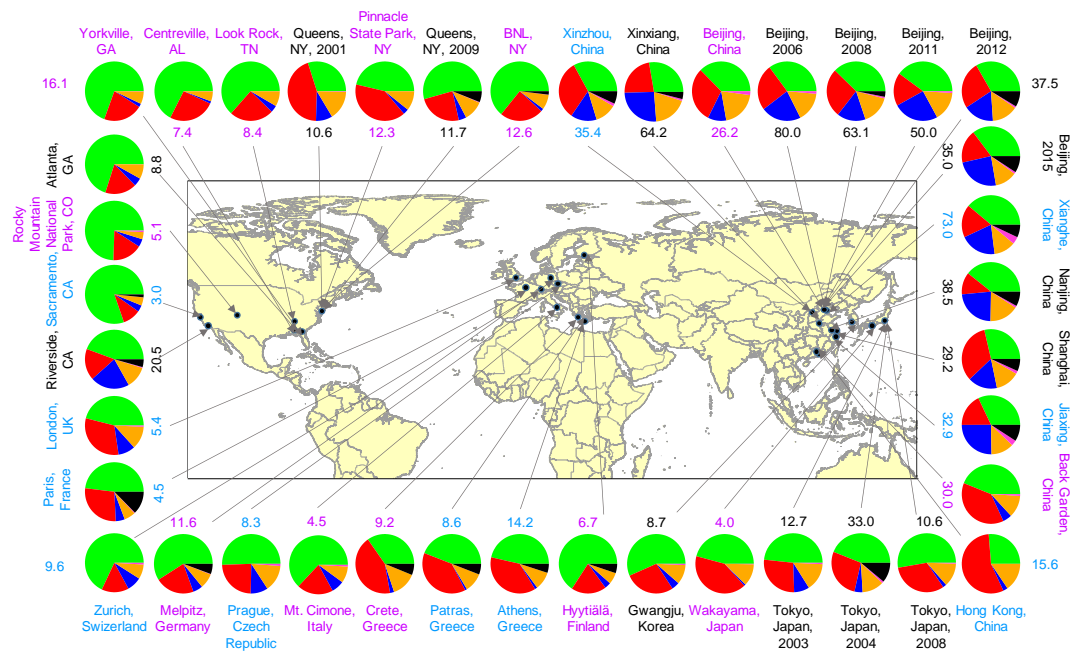


498

499 **Figure 7.** Variations in the nitrate/sulfate mass ratio as a function of (a) temperature (T) and (b) relative humidity (RH). The data were
500 binned according to T and RH, and the mean (cross), median (horizontal line), 25th and 75th percentiles (lower and upper box), and 10th
501 and 90th percentiles (lower and upper whiskers) are shown for each bin.

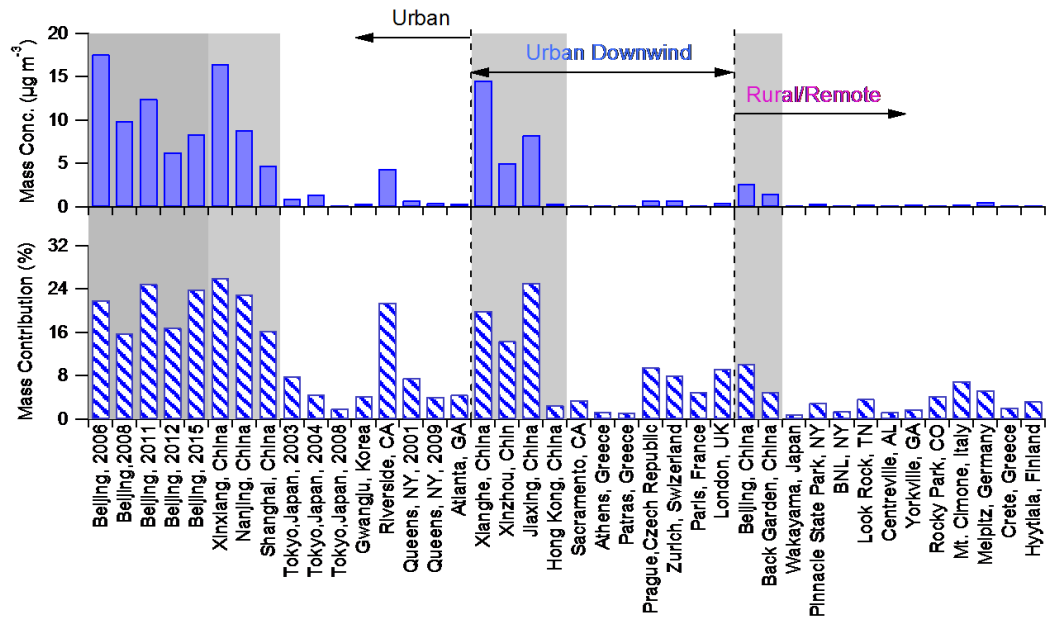


502
503 **Figure 8.** Nitrate/sulfate mass ratios for each cluster. The pie charts represent the average PM₁ chemical composition of the different
504 clusters. In addition, the total PM₁ concentrations for each cluster are also shown.



505

506 **Figure 9.** Summary of the submicron particle measurements in Asia, Europe, and North America (data given in Table S1 in the
 507 supplementary materials). Colors for the study labels indicate the type of sampling location: urban areas (black), urban downwind areas
 508 (blue), and rural/remote areas (pink). The pie charts show the average mass concentration and chemical composition of PM₁ or NR-PM₁:
 509 organics (green), sulfate (red), nitrate (blue), ammonium (orange), chloride (purple), and BC (black).



510

511 **Figure 10.** Average mass concentrations and mass fractions of nitrate at various sampling sites for three types of locations: urban, urban
 512 downwind, and rural/remote areas. Within each category, the sites are ordered from left to right as Asia, North America, and Europe.